Structural and Optical Properties of Ni-Cu Doped TiO₂ Synthesized by Sol-Gel Method

R. Anisha[*, ID] and E.K. Kirupa Vasam[ID]

Department of Chemistry & Research Centre, Nesamony Memorial Christian College (Affiliated to Manonmaniam Sundaranar University, Abishekapatti, Tirunelveli), Marthadam-629165, India

*Corresponding author: E-mail: anisharusselraj@gmail.com

Ni-Cu doped TiO_2 nanoparticles as photocatalyst were synthesized by simple sol-gel method. The effect of Ni and Cu doping on TiO_2 and their structural and optical properties were analyzed by XRD, FT-IR, SEM-EDS, TEM and UV-DRS techniques. The XRD patterns of calcined nanoparticles showed a monophasic anatase structure with average diameter around 8 nm, which is in close agreement with the TEM results. The surface morphology of the prepared Ni-Cu doped TiO_2 nanoparticles were also analyzed by SEM-EDS technique. From UV-DRS analysis, the band-gap energy value of Ni-Cu doped TiO_2 nanoparticles was found to be 2.72 eV. The photocatalytic effect of Ni-Cu doped TiO_2 nanoparticles as photocatalyst was studied under visible light irradiation through the degradation of Congo red azo dye. The photocatalytic results revealed that Ni-Cu doped TiO_2 showed 99.6% degradation efficiency towards Congo red dye, whereas TOC analysis showed a complete mineralization of Congo red dye with minimum degradated byproducts. These results clearly elucidated that the synthesized photocatalyst is practically effective and is recovered easily, thus minimizing the operating costs. Due to the stability of Ni-Cu doped TiO_2 nanoparticles, the prepared photocatalyst exhibit high degrading efficiency even after recycled several times.

Keywords: Doped TiO₂, Photocatalyst, Sol-gel, Congo red, Visible light, Photocatalytic degradation.

INTRODUCTION

Azo dyes are used in various industries such as paper, textile, leather and additives [1]. These industries are releasing a large quantity of wastewater containing toxic dyestuffs into the aquatic systems [2]. These pollutants seriously disturb and destroy the ecological system, leaving a heavy negative impact on both plants and human beings [3]. Many researchers have focused on degradation of dye pollutants and many studies have been developed, such as chlorination [4], electrochemical [5], biodegradation [6], photocatalytic [7-11] and adsorption [12,13] methods. However, advanced oxidation processes are the alternative techniques for the wastewater treatment. The utilization of photocatalysis allows for the safe degradation of organic and inorganic contaminants at ambient temperature and pressure [14]. The most commonly used photocatalysts are TiO_2, CdS, ZnO, FeO_3 and WO_3 [15-21]. Titanium dioxide have some advantages including high thermal and chemical stability, high photocatalytic activity, strong oxidizing power, non-toxic and relatively cost effective. Hence, TiO_2 is mainly used for the degradation of organic pollutants [22-26]. However, due to its large band gap (3.2 eV) its activity is limited to

near-ultraviolet region. To enhance the performance of TiO_2 its structure and morphology is modified by doping with metals and non-metals. Therefore, researchers is of great interest in their research work on the photocatalytic activity of TiO_2 doped with different metal ions such as Fe [27,28], Cu [29,30], Mn [31], Au [32], Ag [33], Ni [34,35] and Pd [36]. The photocatalytic activity of metal doped TiO_2 is dependent on the metal deposition sequence and the type of doped metal [37]. The bimetal photocatalyst exhibit good performance in hydrogen production because these metals act as an electron sink for photoexcitation electron and it extends the photocatalytic activity towards the visible light region [38-40].

In present work, Ni-Cu doped TiO_2 nanoparticles were synthesized by simple sol-gel method with varying wt.% of nickel and copper and its application on degradation of Congo red dye in water using solar light and to evaluate the complete degree of degradation of dye as well as its stability and recyclability.

EXPERIMENTAL

Characterization: The particle size and phase structure of the prepared photocatalyst were analyzed using powder XRD

with CuKα radiation (λ = 1.5406 Å) as an incident beam in the 2θ mode over a range of 20-80º operated at 40 kV and 30 mA. The presence of functional groups in the photocatalyst was identified by FT-IR technique using Jasco FTIR-4600, Japan (AVATAR 370). The band gap energy and absorption edge were investigated using DRS analysis (Agilent Cary 5000) and BaSO₄ as reference. The surface morphology along with its elemental composition was analyzed by SEM (FEI Quanta FEG 200F) equipped with an energy dispersive X-ray (EDS) spectrophotometer operated at 30 kV and HR-TEM (JEOL-2100) with an accelerating voltage of 200 kV.

Preparation of Ni-Cu doped TiO₂ particle: The Ni-Cu doped TiO₂ photocatalyst was prepared by sol-gel method. In this method, titanium tetraisopropoxide (TIP) acted as the precursor of titanium. The photocatalyst was prepared by mixing 2.5 mL of deionized water with 10 mL of isopropanol. The above solution was stirred for 0.5 h. To this solution, required quantity of 0.5 M TIP was added dropwise to form a suspension followed by the addition of 1 mL of conc. HNO₃. The solution was vigorously stirred for 45 min. Finally, nickel nitrate hexahydrate and copper nitrate trihydrate of desired concentration were added dropwise with continuous stirring. The obtained gel was dried at 80 ºC for 5 h and then annealed at 450 ºC for 3 h to get Ni-Cu doped TiO₂ photocatalyst [41].

Photocatalytic activity: The photodegradation efficiency of the synthesized Ni-Cu doped TiO₂ nanoparticles were evaluated by degradation of Congo red dye as contaminant. The Ni-Cu doped TiO₂ nanoparticles (250 mg) was immersed in 100 mL of 20 ppm Congo red dye solution in a beaker. The solution was allowed to equilibrate completely for 30 min in dark using magnetic stirrer. Then, the system was irradiated using visible light and then 2 mL suspension of Congo red was withdrawn and analyzed at 10 min interval at λ_{max} = 500 nm, which corresponds to the maximum absorbance of dye. The percentage of degradation was calculated using eqn. 1:

$$\text{Degradation (\%)} = \frac{C_o - C_t}{C_o} \times 100 \qquad (1)$$

where, C_o is the initial concentration of Congo red, C_t is the final concentration of Congo red after visible light irradiation.

RESULTS AND DISCUSSION

XRD analysis: The phase structure and the crystal size of the synthesized photocatalyst were determined by using XRD analysis. Fig. 1 shows the XRD patterns of undoped TiO₂ and Ni-Cu doped TiO₂. In Fig. 1b, the synthesized Ni-Cu TiO₂ shows the presence of pure anatase crystal planes as (101), (112), (200), (105), (204), (116) and (215) (JCPDS No. 21-1272). There were no peaks corresponding to nickel and copper oxide in Ni-Cu doped TiO₂ which is attributed to low concentration or elegant diffusion of Ni²⁺ and Cu²⁺ into TiO matrix [42,43]. Since the ionic radii of Ni²⁺ (0.69 Å) and Cu²⁺ (0.73 Å) are greater than that of Ti⁴⁺ (0.61 Å), the addition of dopants does not alter the phase of host TiO₂ nanoparticle, but it does cause a shift in the (101) peak towards the lower angle. The average crystallite size of the samples was calculated by Debye-Scherrer's formula:

$$D = \frac{K\lambda}{\beta \cos\theta} \qquad (2)$$

where D represents the average crystalline size, 0.9 indicates the shape factor of grain, λ corresponds to wavelength of X-ray, β gives the FWHM of diffraction peak and θ is the incident angle of X-ray. The average calculated crystal size of the Ni-Cu doped TiO₂ was found to be 8 nm.

FT-IR analysis: FT-IR spectra of undoped and Ni-Cu doped TiO₂ samples are shown in Fig. 2. The peaks at 3400 and 1628 cm⁻¹ corresponds to stretching and bending vibrations of H₂O and OH⁻, respectively. The lower wavelength band around 437 cm⁻¹ is due to the bending vibration of M-O such as Ti-O and Ti-O-Ti framework bonds [44]. When comp-ared to the undoped TiO₂, most of the peaks in Ni-Cu doped TiO₂ showed a slight shift in the bands, since the dopants are located in the interstitial space of lattice.

SEM-EDAX studies: The SEM images of Ni-Cu doped TiO₂ showed the agglomeration of uniform particles when compared to TiO₂ (Fig. 3). This revealed that co-doping of Ni²⁺ and Cu²⁺ did not affect the morphology of TiO₂ which is attributed to the small amount of Ni²⁺ and Cu²⁺ ions incorporated into the TiO₂ matrix [45-47]. EDAX spectrum (Fig. 4) shows the atomic % Ni-Cu TiO₂ chemical composition in the synthesized Ni-Cu doped TiO₂ nanoparticles, which confirmed
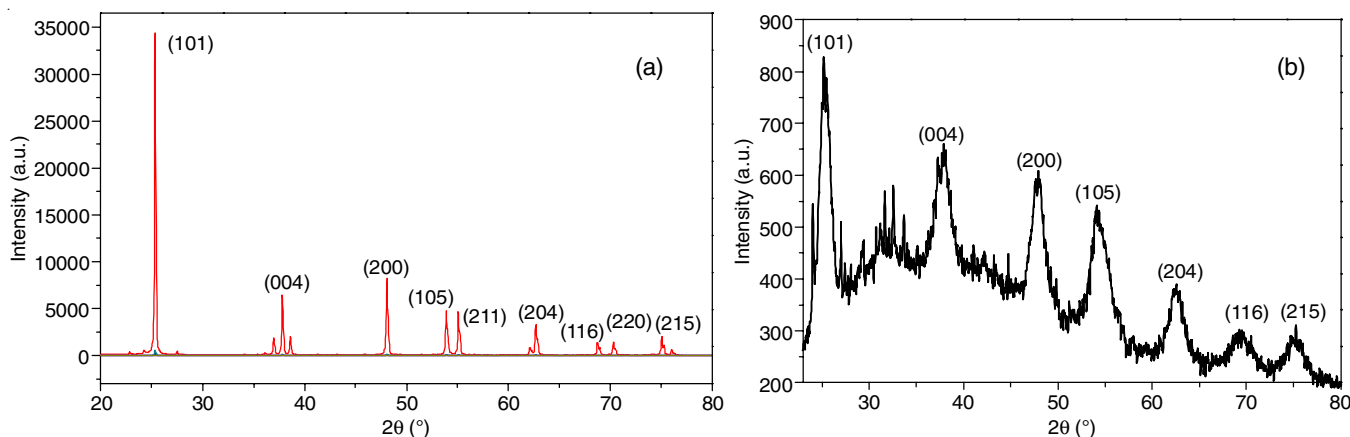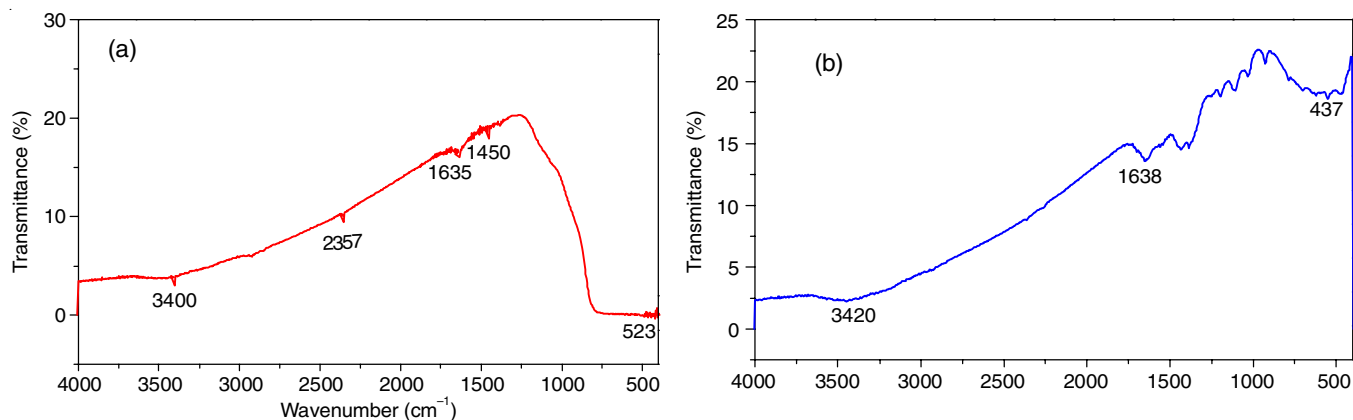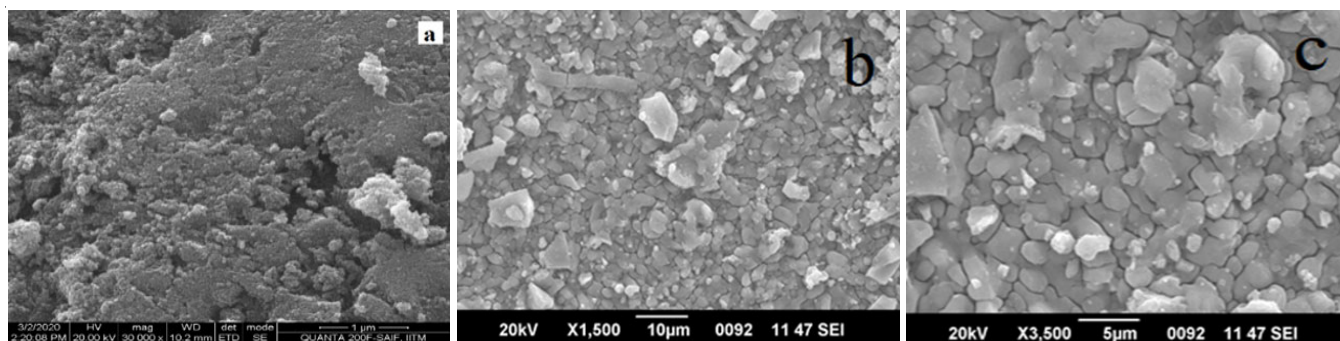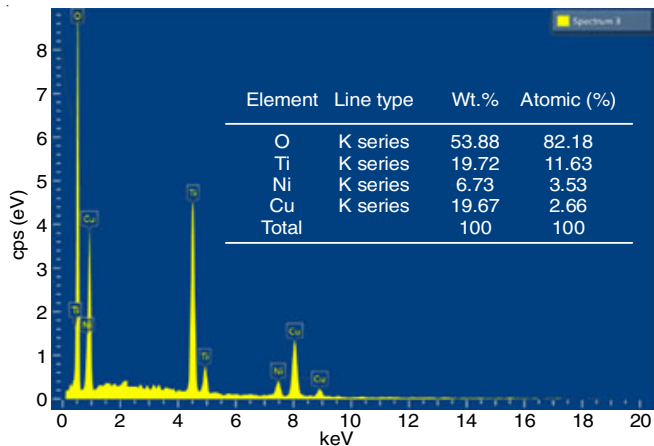

Fig. 1. XRD patterns of (a) TiO₂ (b) Ni-Cu doped TiO₂

Fig. 2. FT-IR spectra of (a) TiO₂ (b) Ni-Cu doped TiO₂

Fig. 3. SEM images of (a) undoped TiO₂ (b and c) Ni-Cu doped TiO₂

Element	Line type	Wt.%	Atomic (%)
O	K series	53.88	82.18
Ti	K series	19.72	11.63
Ni	K series	6.73	3.53
Cu	K series	19.67	2.66
Total		100	100

Fig. 4. EDAX spectrum of Ni-Cu doped TiO₂ nanoparticles

the presence of Ti, O, Ni and Cu in the TiO₂ lattice. Doping of Cu-Ni with TiO₂ with has not affected the morphological appearance due to very small concentration of dopants incorporated in the lattice of TiO₂.

TEM studies: The structure of the doped TiO₂ was further investigated by HR-TEM images. Fig. 5 shows that Ni-Cu doped TiO₂ nano catalyst were found to be spherical in shape. From the high-resolution TEM images, the lattice fringes with inter planar distance of 0.35 and 0.18 nm were observed, which corresponds to the (101) and (200) planes of anatase TiO₂ respectively [48,49]. It indicates that the synthesized Ni-Cu doped TiO₂ has crystalline structure. The particle size distribution histogram (Fig. 5e) obtained by Gaussian fitting method

confirmed that the average particle size of Ni-Cu doped TiO₂ is 8 nm.

Optical studies: The UV absorption spectra of the samples showed a band edge of 500 nm for Ni-Cu doped TiO₂ (Fig. 6a), which in turn showed a possible enhancement in the photocatalytic activity of Ni-Cu doped TiO₂. From Fig. 6b, the band gap energy value for Ni-Cu doped TiO₂ was found to be 2.72 eV. Due to the doping of TiO₂ with Ni^{2+} and Cu^{2+}, the electrons involved in transitions could not be transferred directly to the conduction band of TiO₂. The reason behind this is that the s-d transition states of the dopants Ni^{2+}, Cu^{2+} and oxygen vacancies capture the transition electrons. Therefore, the sub band states formed by Ni^{2+}, Cu^{2+} and oxygen vacancies significantly contribute to lowering the bad-gap values in comparison to TiO₂. This decrease in band gap, increases the photocatalytic behaviour of Ni-Cu doped TiO₂ [50].

Photocatalytic degradation studies: The UV spectra of Congo red dye solution (20 ppm) with Ni-Cu doped TiO₂ (250 mg) photocatalyst as a function of time irradiated in the presence of visible light is shown in Fig. 7. Initially, Congo red dye with photocatalyst exhibited a maximum absorption at λ_{max} = 500 nm and this maximum absorbance gradually decreased with increase in the irradiation time and therefore confirmed that the toxic dye was successfully degraded by using Ni-Cu doped TiO₂ photocatalyst.

Mechanism: From the investigation of degradation of Congo red dye with Ni-Cu doped TiO₂, it was found that the high surface area and the retardation of electron-hole recombination centres is the basic process for the photocatalysis of
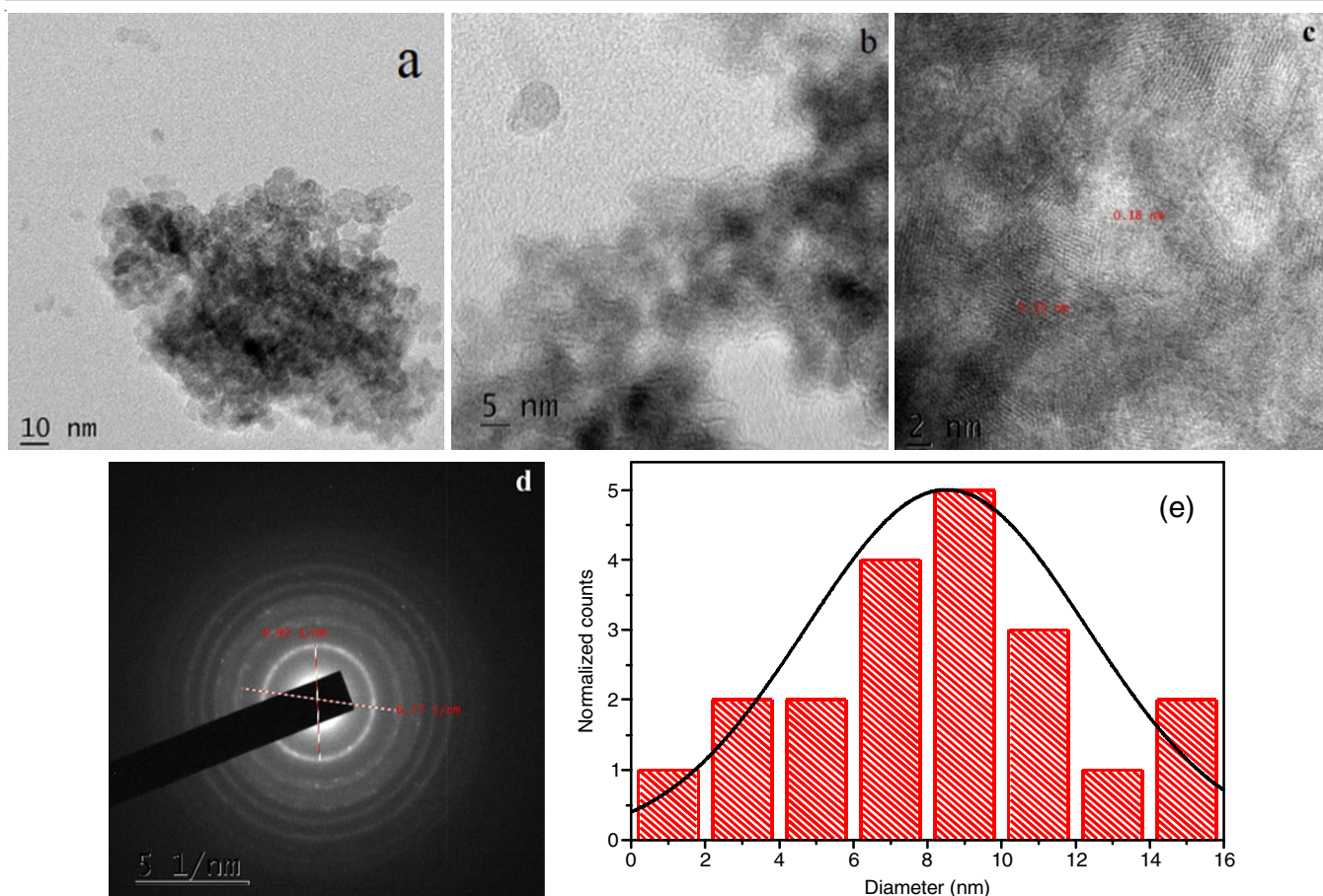
Fig. 5. (a,b) TEM images of Ni-Cu doped TiO₂, (c) HRTEM images of Ni-Cu doped TiO₂, (d) SAED pattern of Ni-Cu doped TiO₂, (e) particle size distribution of Ni-Cu doped TiO₂
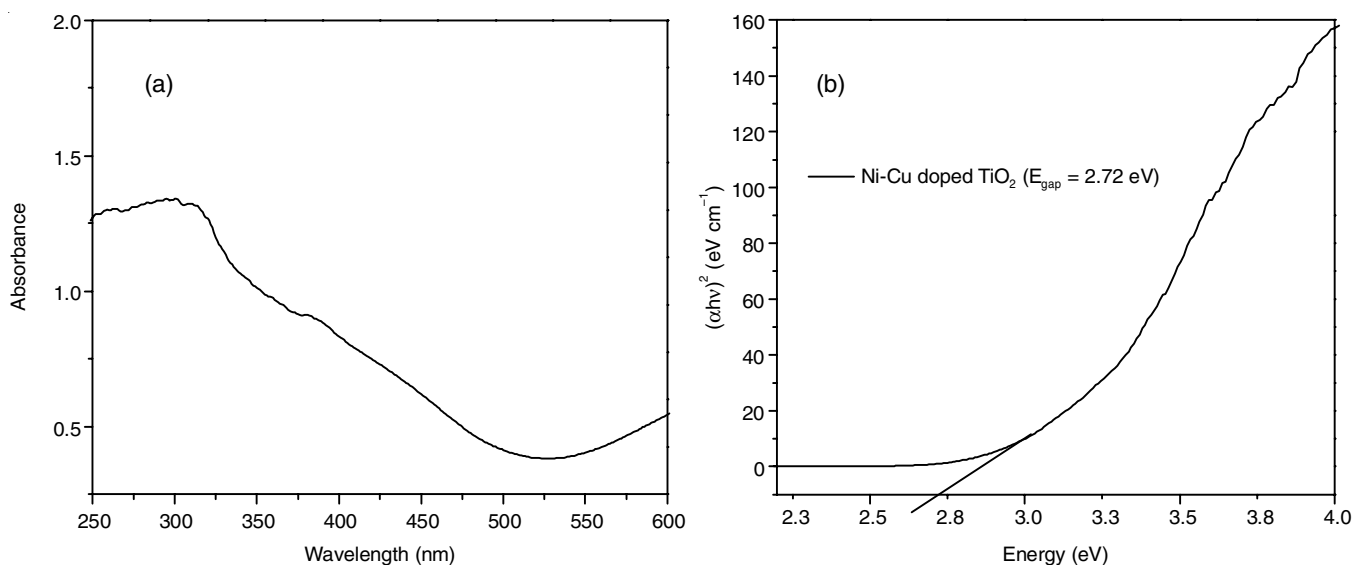

Fig. 6. (a) UV-vis absorption spectra of Ni-Cu doped TiO₂ (b) Optical band gap (E_g) spectra of Ni-Cu doped TiO₂

organic compounds by photocatalyst. The generated electrons were attracted towards the metal particle. The photogenerated holes react with OH^- or H_2O, oxidize into OH radicals, resulting in the degradation of organic compounds adsorbed onto the TiO₂ surface. As a result, the Ni-Cu doped TiO₂ not only increases visible light absorption due to a narrowing band gap, but also improves the efficiency with which photoinduced electrons and holes are separated.

Photocatalytic mineralization of Congo red dye: Photocatalytic degradation of Congo red was also confirmed by COD analysis before and after the experiment. The COD of the dye solution before (20155.2 mg/L) and after (92.43
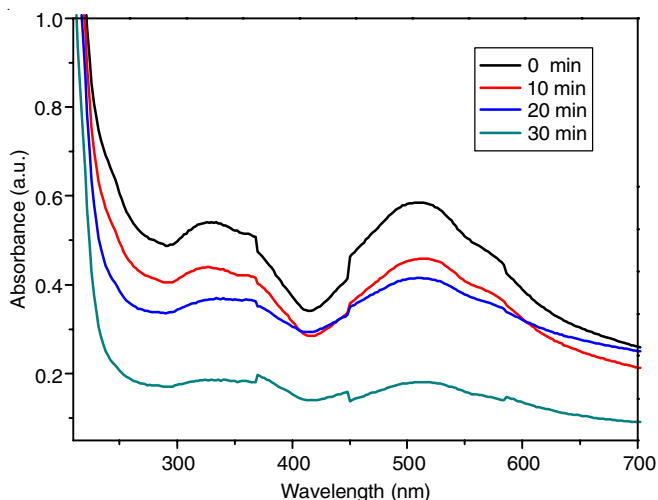
Fig. 7.   UV-absorption spectra of dye under visible light by using la doped TiO$_2$

mg/L), the irradiation using visible light was measured. the reduction in the COD values of dye solution confirmed that all the dye molecules had been mineralized and the colour had been eliminated from the solution.

The % of mineralization was calculated by using eqn. 3:

$$\text{Mineralization (\%)} = \frac{COD_o - COD_t}{COD_o} \times 100 \qquad (3)$$

Reusability: In order to analyze the reusability of Ni-Cu doped TiO$_2$, photocatalyst after the degradation experiments was filtered from the reaction medium, washed with deionized water for several times and dried under normal temperature. After drying, it was utilized to perform more number of photocatalytic degradation experiments on Congo red, under same experimental conditions. The Ni-Cu doped TiO$_2$ nanoparticles, exhibited stable photocatalytic performance without any change in the degradation efficiency for about four cycles and then the efficiency decreased slightly for the next immediate cycles (Fig. 8). This performance has exhibited an excellent long-term stability and good potentiality of the prepared photocatalyst for wastewater treatment applications.
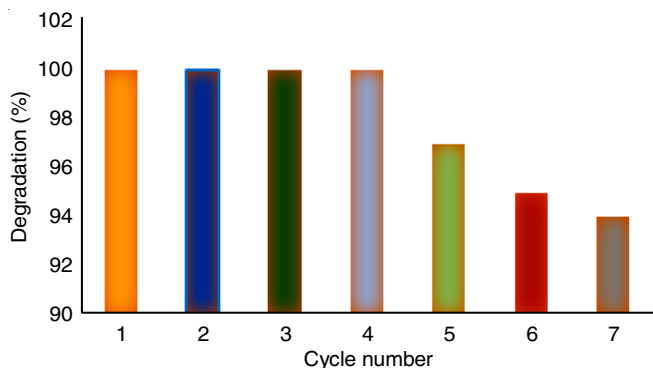

Fig. 8. Recycling ability of catalyst

Conclusion

A novel photocatalyst Ni-Cu doped TiO$_2$ with size 8 nm was successfully synthesized by a simple sol-gel method with low-cost precursors to degrade contaminants in aqueous solutions. The FT-IR results confirmed the presence of Ni and Cu in the lattice structure of TiO$_2$. The co-doping of TiO$_2$ with transition metals has led to small grain size, low band gap, high surface area and enhanced the photocatalytic activity of catalyst. It was suggested that the doping of Ni-Cu on TiO$_2$ enables an impurity band to develop between the valence band and conduction band, hence increasing the photocatalytic activity of the material. Thus, Ni-Cu doped TiO$_2$ was found to be an efficient photocatalyst for degradation of Congo red dye within 30 min. The TOC results showed a high degree of mineralization of Congo red dye achieved using Ni-Cu doped TiO$_2$ nano photocatalyst. Thus, Ni-Cu doped TiO$_2$ exhibited a good recyclability and stability under solar light irradiation.

CONFLICT OF INTEREST

The authors declare that there is no conflict of interests regarding the publication of this article.

REFERENCES

1. M. Dakiky and I. Nemcova, *Dyes Pigments*, **44**, 181 (2000);
   https://doi.org/10.1016/S0143-7208(99)00086-8
2. M. Vautier, C. Guillard and J.M. Herrmann, *J. Catal.*, **201**, 46 (2001);
   https://doi.org/10.1006/jcat.2001.3232
3. X.H. Li, Y. Wu, Y.H. Shen, Y. Sun, Y. Yang and A. Xie, *Appl. Surf. Sci.*, **427**, 739 (2018);
   https://doi.org/10.1016/j.apsusc.2017.08.091
4. S. Yaparatne, C.P. Tripp and A. Amirbahman, *J. Hazard. Mater.*, **346**, 208 (2018);
   https://doi.org/10.1016/j.jhazmat.2017.12.029
5. S. Kumar, B. Ahmed, A.K. Ojha, J. Das and A. Kumar, *Mater. Res. Bull.*, **90**, 224 (2017);
   https://doi.org/10.1016/j.materresbull.2017.02.044
6. C. Yang, J.S. Yu, Q.S. Li and Y.M. Yu, *Mater. Res. Bull.*, **87**, 72 (2017);
   https://doi.org/10.1016/j.materresbull.2016.11.024
7. S. Guo, S. Han, H. Mao, S. Dong, C. Wu, L. Jia, B. Chi, J. Pu and J. Li, *J. Power Sources*, **245**, 979 (2014);
   https://doi.org/10.1016/j.jpowsour.2013.07.044
8. S. Guo, T. Zhao, Z. Jin, X. Wan, P. Wang, J. Shang and S. Han, *J. Power Sources*, **293**, 17 (2015);
   https://doi.org/10.1016/j.jpowsour.2015.05.042
9. S.Y. Guo, S. Han, B. Chi, J. Pu and J. Li, *ACS Appl. Mater. Interfaces*, **6**, 4743 (2014);
   https://doi.org/10.1021/am4054095
10. S. Guo, S. Han, H. Mao, C. Wu, L. Jia, B. Chi, J. Pu and L. Jian, *J. Alloys Compd.*, **544**, 50 (2012);
    https://doi.org/10.1016/j.jallcom.2012.07.128
11. A.A. Ismail, I. Abdelfattah, M. Faisal and A. Helal, *Hazard. Mater*, **342**, 519 (2018);
    https://doi.org/10.1016/j.jhazmat.2017.08.046
12. L.-N. Liu, J.-G. Dai, T.-J. Zhao, S.-Y. Guo, D.-S. Hou, P. Zhang, J. Shang, S. Wang and S. Han, *RSC Adv.*, **7**, 35075 (2017);
    https://doi.org/10.1039/C7RA04259K
13. D. Zhao, G. Sheng, C. Chen and X. Wang, *Appl. Catal. B*, **111-112**, 303 (2012);
    https://doi.org/10.1016/j.apcatb.2011.10.012
14. M.A. Fox and M.T. Dulay, *Chem. Rev.*, **93**, 341 (1993);
    https://doi.org/10.1021/cr00017a016
15. M.H. Habibi, A. Hassanzadeh and S. Mahdavi, *J. Photochem. Photobiol. Chem.*, **172**, 89 (2005);
    https://doi.org/10.1016/j.jphotochem.2004.11.009
16. S. Chakrabarti and B.K. Dutta, *J. Hazard. Mater. B*, **112**, 269 (2004);
    https://doi.org/10.1016/j.jhazmat.2004.05.013
17. M. Movahedi, A.R. Mahjoub and S. Janitabar-Darzi, *J. Iran. Chem. Soc.*, **6**, 570 (2009);
    https://doi.org/10.1007/BF03246536

18. R.K. Wahi, W.W. Yu, Y. Liu, M.L. Mejia, J.C. Falkner, W. Nolte and V.L. Colvin, *J. Mol. Catal. A: Chemical*, **242**, 48 (2005); https://doi.org/10.1016/j.molcata.2005.07.034

19. J. Bandara, J.A. Mielczarski and J. Kiwi, *Langmuir*, **15**, 7680 (1999); https://doi.org/10.1021/la990030j

20. V. Feng, X. Hu, P.L. Yue, H.Y. Zhu and G.Q. Lu, *Ind. Eng. Chem. Res.*, **42**, 2058 (2003); https://doi.org/10.1021/ie0207010

21. S. Nam and P.G. Tratnyyek, *Water Res.*, **34**, 1837 (2000); https://doi.org/10.1016/S0043-1354(99)00331-0

22. M.M. Joshi, N.K. Labhsetwar, P.A. Mangrulkar, S.N. Tijare, S.P. Kamble and S.S. Rayalu, *Appl. Catal. A Gen.*, **357**, 26 (2009); https://doi.org/10.1016/j.apcata.2008.12.030

23. E.M. Neville, M.J. Mattle, D. Loughrey, B. Rajesh, J.M.D. MacElroy, J.A. Sullivan and K.R. Thampi, *J. Phys. Chem. C*, **116**, 16511 (2012); https://doi.org/10.1021/jp303645p

24. A. Orendorz, A. Brodyanski, J. Losch, L.H. Bai, Z.H. Chen, Y.K. Le, C. Ziegler and H. Gnaser, *Surf. Sci.*, **601**, 4390 (2007); https://doi.org/10.1016/j.susc.2007.04.127

25. N. Zhao, Y. Yao, J.J. Feng, M.M. Yao and F. Li, *Water Air Soil Pollut.*, **223**, 5855 (2012); https://doi.org/10.1007/s11270-012-1321-3

26. K. Dedkova, J. Lang, K. Matejova, P. Peikertova, J. Holesinsky, V. Vodarek and J. Kukutschova, *J. Photochem. Photobiol. B*, **149**, 265 (2015); https://doi.org/10.1016/j.jphotobiol.2015.06.018

27. B. Peng, X. Meng, F. Tang, X. Ren, D. Chen and J. Ren, *J. Phys. Chem. C*, **113**, 20240 (2009); https://doi.org/10.1021/jp906937e

28. T.K. Ghorai, S.K. Biswas and P. Pramanik, *Appl. Surf. Sci.*, **254**, 7498 (2008); https://doi.org/10.1016/j.apsusc.2008.06.042

29. X. Qlu, M. Miyauchi, K. Sunada, M. Minoshima, M. Liu, Y. Lu, Y. Lu, D. Li, Y. Shimodaira, Y. Hosogi, Y. Kuroda and K. Hashimoto, *ACS Nano*, **6**, 1609 (2012); https://doi.org/10.1021/nn2045888

30. T. Ghorai, *Open J. Phys. Chem.*, **1**, 28 (2011); https://doi.org/10.4236/ojpc.2011.12005

31. T.K. Ghorai, S. Pramanik and P. Pramanik, *Appl. Surf. Sci.*, **255**, 9026 (2009); https://doi.org/10.1016/j.apsusc.2009.06.086

32. S.T. Kochuveedu, D. Kim and D.H. Kim, *J. Phys. Chem. C*, **116**, 2500 (2012); https://doi.org/10.1021/jp209520m

33. H. Zhang, C. Liang, J. Liu, Z. Tian, G. Wang and W. Cai, *Langmuir*, **28**, 3938 (2012); https://doi.org/10.1021/la2043526

34. M. Karimipour, J.M. Wikberg, V. Kapaklis, N. Shahtahmasebi, M.R.R. Abad, M. Yeganeh, M.M. Bagheri-Mohagheghi and P. Svedlindh, *Phys. Scr.*, **84**, 035702 (2011); https://doi.org/10.1088/0031-8949/84/03/035702

35. J. Li, F. Meng, S. Suri, W. Ding, F. Huang and N. Wu, *Chem. Commun.*, **48**, 8213 (2012); https://doi.org/10.1039/c2cc30376k

36. Z. Zhang, Y. Yu and P. Wang, *ACS Appl. Mater. Interfaces*, **4**, 990 (2012); https://doi.org/10.1021/am201630s

37. A. Malankowska, M.P. Kobylanski, A. Mikolajczyk, G. Nowaczyk, O. Cavdar, M. Jarek, W. Lisowski, M. Michalska, E. Kowalska, B. Ohtani and A. Zaleska-Medynska, *ACS Sustain. Chem. Eng.*, **6**, 16665 (2018); https://doi.org/10.1021/acssuschemeng.8b03919

38. S. Hara, M. Yoshimizu, S. Tanigawa, L. Ni, B. Ohtani and H. Irie, *J. Phys. Chem. C*, **116**, 17458 (2012); https://doi.org/10.1021/jp306315r

39. A.L. Luna, E. Novoseltceva, E. Louarn, P. Beaunier, E. Kowalska, B. Ohtani, M.A.Valenzuela, H. Remita and C. Colbeau-Justina, *Appl. Catal. B*, **191**, 18 (2016); https://doi.org/10.1016/j.apcatb.2016.03.008

40. M.G. Mendez-Medrano, E. Kowalska, A. Lehoux, A. Herissan, B. Ohtani, S. Rau, C. Colbeau-Justin, J.L. Rodriguez-Lopez and H. Remita, *J. Phys. Chem.*, **120**, 5143 (2016); https://doi.org/10.1021/acs.jpcc.5b10703

41. T. Raguram and K.S. Rajni, *Appl. Phys., A Mater. Sci. Process.*, **125**, 288 (2019); https://doi.org/10.1007/s00339-019-2581-1

42. K.H. Yoon, J.S. Noh, C.H. Kwon and M. Muhammed, *Mater. Chem. Phys.*, **95**, 79 (2006); https://doi.org/10.1016/j.matchemphys.2005.06.001

43. M. Yan, F. Chen, J. Zhang and M. Anpo, *J. Phys. Chem. B*, **109**, 8673 (2005); https://doi.org/10.1021/jp046087i

44. M. Picquart, L. Escobaralarcon, E. Torres, E. Haroponiatowski and T. Lopez, *J. Mater. Sci.*, **37**, 3241 (2002); https://doi.org/10.1023/A:1016126832567

45. M.M. Momeni, Y. Ghayeb and F. Ezati, *J. Colloid Interface Sci.*, **514**, 70 (2018); https://doi.org/10.1016/j.jcis.2017.12.021

46. S. Challagulla, K. Tarafder, R. Ganesan and S. Roy, *J. Phys. Chem. C*, **121**, 27406 (2017); https://doi.org/10.1021/acs.jpcc.7b07973

47. J. Zhao, Y. Yang, Y. Li, L. Zhao, H. Wang, G. Song and G. Tang, *Sol. Energy Mater. Sol. Cells*, **168**, 62 (2017); https://doi.org/10.1016/j.solmat.2017.04.014

48. H. Zhao, Y. Wu, H. Nan, Y. Du, G. Yang, G. Wang, H. Chen, H. Wei and H. Lin, *Mater. Res. Express*, **6**, 085020 (2019); https://doi.org/10.1088/2053-1591/ab1c2a

49. Q. Li, R. Liu, T. Wang, K. Xu, Q. Dong, B. Liu, J. Liu and B. Liu, *AIP Adv.*, **5**, 097128 (2015); https://doi.org/10.1063/1.4930916

50. B. Choudhury, M. Dey and A. Choudhury, *Int. Nano Lett.*, **3**, 25 (2013); https://doi.org/10.1186/2228-5326-3-25